

Is shrub expansion into grasslands pushed or pulled?  
A spatial integral projection model for woody plant  
encroachment

Trevor Drees<sup>a</sup>, Brad M. Ochocki<sup>b</sup>, Scott L. Collins<sup>c</sup>, and Tom E.X. Miller<sup>b</sup>

<sup>a</sup>Department of Biology, Penn State University, State College, PA USA

<sup>b</sup>Program in Ecology and Evolutionary Biology, Department of BioSciences, Rice  
University, Houston, TX USA

<sup>c</sup>Department of Biology, University of New Mexico, Albuquerque, NM USA

August 4, 2022

## Abstract

<sup>1</sup>The<sup>1</sup> encroachment of woody plants into grasslands is a global phenomenon with implications for biodiversity and ecosystem function. Understanding and predicting the pace of expansion and the underlying processes that control it are key challenges in the study and management of woody encroachment. Theory from spatial population biology predicts that the occurrence and speed of population expansion should depend sensitively on the nature of conspecific density dependence. Positive feedbacks of shrub encroachment should generate positive density dependence (Allee effects) and thus pushed-wave dynamics. We studied the spatial dynamics of creosote bush (*Larrea tridentata*), which has a record of encroachment into Chihuahuan Desert grassland. We used observational data and seedling transplant experiments to test the strength and direction of density dependence in shrub demographic performance along a gradient of shrub density at the grass-shrub ecotone. We also used seed-drop experiments and wind data to construct a mechanistic (WALD) dispersal kernel, which provides insight into how far wind can carry creosote seeds. Combining demography and dispersal data, a spatial integral projection model predicting that, contrary to expectations based on potential for positive feedbacks, the shrub encroachment wave is “pulled” by maximum fitness at the low-density front. However, the predicted pace of expansion was strikingly slow (ca. 8 cm/yr), and this prediction was supported by independent re-surveys of the ecotone showing little to no change in spatial extent of shrub cover over 12 years. Encroachment speed was acutely sensitive to seedling recruitment, suggesting that this population may be primed for pulses of expansion under conditions that are favorable for recruitment. Our integration of observations, experiments, and modeling reveals not only that this

---

<sup>1</sup>first draft – will need to be tailored to length limit of target journal

24 ecotone is effectively stationary under current conditions, but also *why* that is so and  
25 how that may change as the environment changes.

## 26 **Keywords**

27 density-dependence, ecotones, woody encroachment, shrubs, integral projection model,  
28 dispersal, Allee effects

## Introduction

The recent and ongoing encroachment of shrubs and other woody plants into adjacent grasslands has caused significant vegetation changes across arid and semi-arid landscapes worldwide (Cabral et al., 2003; Gibbens et al., 2005; Goslee et al., 2003; Parizek et al., 2002; Roques et al., 2001; Trollope et al., 1989; Van Auken, 2009, 2000). The process of encroachment generally involves increases in the number or density of woody plants in both time and space (Van Auken, 2000), which can drive shifts in plant community structure and alter ecosystem processes (Knapp et al., 2008; Ravi et al., 2009; Schlesinger and Pilmanis, 1998; Schlesinger et al., 1990). Other effects of encroachment include changes in ecosystem services (Kelleway et al., 2017; Reed et al., 2015), declines in biodiversity (Brandt et al., 2013; Ratajczak et al., 2012; Sirami and Monadjem, 2012), and economic losses in areas where the proliferation of shrubs adversely affects grazing land and pastoral production (Mugasi et al., 2000; Oba et al., 2000).

Woody plant encroachment can be studied through the lens of spatial population biology as a wave of individuals that may expand across space and over time (Kot et al., 1996; Neubert and Caswell, 2000; Pan and Lin, 2012; Wang et al., 2002). Theory predicts that the speed of wave expansion depends on two processes: local demography and dispersal of propagules. First, local demographic processes include recruitment, survival, growth, and reproduction, which collectively determine the rate at which newly colonized locations increase in density and produce new propagules. Second, colonization events are driven by the spatial dispersal of propagules, which is commonly summarized as a probability distribution of dispersal distance, or “dispersal kernel”. The speed at which expansion waves move is highly dependent upon the shape of the dispersal kernel, especially long-distance dispersal events in the tail of the distribution (Skarpaas

53 and Shea, 2007). Both demography and dispersal may depend on plant size, since larger  
54 plants often have improved demographic performance and release seeds from greater  
55 heights, leading to longer dispersal distances (Nathan et al., 2011). Accounting for popu-  
56 lation structure, including size structure, may therefore be important for understanding  
57 and predicting wave expansion dynamics (Neubert and Caswell, 2000).

58 Theory predicts that the nature of conspecific density dependence is another crit-  
59 ical feature of expansion dynamics but this is rarely studied in the context of woody  
60 plant encroachment. Expansion waves typically correspond to gradients of conspecific  
61 density – high in the back and low at the front – and demographic rates may be sen-  
62 sitive to density due to intraspecific interactions like competition or facilitation. If the  
63 demographic effects of density are strictly negative due to competitive effects that in-  
64 crease with density then demographic performance is maximized as density goes to  
65 zero, at the leading edge of the wave. Under these conditions, the wave is “pulled” for-  
66 ward by individuals at the low-density vanguard (Kot et al., 1996), and targeting these  
67 individuals and locations would be the most effective way to slow down or prevent en-  
68 croachment. However, woody encroachment systems often involve positive feedbacks  
69 whereby shrub establishment modifies the environment in ways that facilitate further  
70 shrub recruitment. For example, woody plants can modify their micro-climates in ways  
71 that elevate nighttime minimum temperatures, promoting conspecific recruitment and  
72 survival for freeze-sensitive species (D’Odorico et al., 2010; Huang et al., 2020). Posi-  
73 tive density dependence (or Allee effects) causes demographic rates to be maximized at  
74 higher densities behind the leading edge, which “push” the expansion forward, leading  
75 to qualitatively different expansion dynamics (Keitt et al., 2001; Kot et al., 1996; Lewis  
76 and Kareiva, 1993; Sullivan et al., 2017; Taylor and Hastings, 2005; Veit and Lewis, 1996).  
77 Pushed expansion waves generally have different shapes (steeper density gradients) and

78 slower speeds than pulled waves (Gandhi et al., 2016), and may require different strate-  
79 gies for managing or decelerating expansion (Taylor and Hastings, 2005). The potential  
80 for positive feedbacks is well documented in woody encroachment systems as a key fea-  
81 ture of bi-stability (the existence of woody and herbaceous habitats as alternative stable  
82 states: Wilcox et al. (2018)) but it remains unclear whether and how strongly these feed-  
83 backs decelerate shrub expansion and influence strategies for management of woody  
84 encroachment.

85 In this study, we linked woody plant encroachment to ecological theory for spreading  
86 populations, with the goals of understanding how seed dispersal and density-dependent  
87 demography drive encroachment, and determining whether the encroachment wave is  
88 pushed or pulled. Throughout the aridlands of the southwestern United States, shrub  
89 encroachment into grasslands is well documented (D’Odorico et al., 2012) but little is  
90 known about the dispersal and demographic processes that govern it. Our work fo-  
91 cused on encroachment of creosotebush (*Larrea tridentata*) in the northern Chihuahuan  
92 Desert. Expansion of this species into grasslands over the past 150 years has been well  
93 documented, leading to decreased cover of *Bouteloua eriopoda*, the dominant foundation  
94 species of Chihuahuan desert grassland (Buffington and Herbel, 1965; Gardner, 1951;  
95 Gibbens et al., 2005). As in many woody encroachment systems, creosotebush expansion  
96 generates ecotones marking a transition from dense shrubland to open grassland, with a  
97 transition zone in between where shrubs can often be found interspersed among grasses  
98 (Fig. 1).

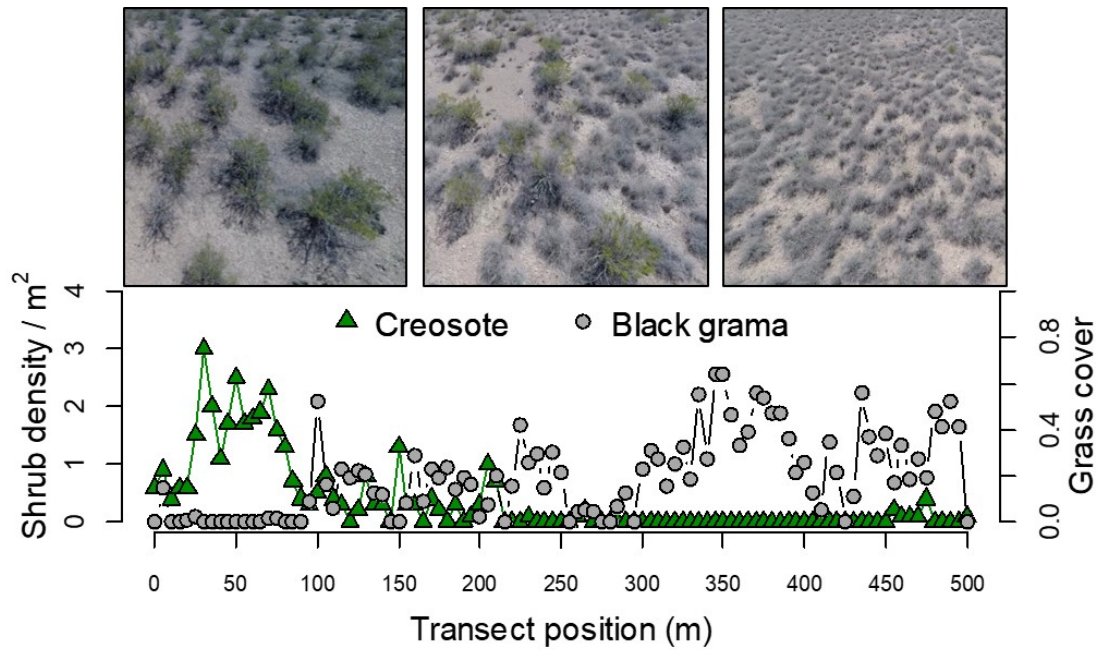


Figure 1: Example of an ecotone transect at Sevilleta LTER, spanning gradients of creosotebush and black grama grass.

99 Historically, creosotebush encroachment into grasslands is believed to have been  
 100 driven by a combination of factors including overgrazing, drought, variability in rain-  
 101 fall, and suppression of fire regimes Moreno-de las Heras et al. (2016). These shrubs  
 102 are also thought to further facilitate their own encroachment through positive feedbacks  
 103 (D’Odorico et al., 2012; Grover and Musick, 1990) by modifying their environment in  
 104 ways that favor continued growth and recruitment, including changes to the local micro-  
 105 climate (D’Odorico et al., 2010) and rates of soil erosion (Turnbull et al., 2010). Such pos-  
 106 itive feedback also involve suppression of herbaceous competitors, reducing competition  
 107 as well as the amount of flammable biomass used to fuel the fires that keep creosotebush  
 108 growth in check (Van Auken, 2000). We hypothesized that, given potential for positive

109 feedback mechanisms, the rarity of conspecifics at the low-density encroachment front  
110 may depress demographic performance and generate pushed-wave dynamics.

111 We used a combination of observational and experimental data from shrub ecotones  
112 in central New Mexico to parameterize a spatial integral projection model (SIPM) that  
113 predicts that speed of encroachment ( $m/yr$ ) resulting from lower-level demographic and  
114 dispersal processes. Our data came from demographic surveys and experimental trans-  
115 plants along replicate ecotone transects spanning a gradient of shrub density, and seed  
116 drop experiments to estimate the properties of the dispersal kernel. We focused on wind  
117 dispersal of seeds, since little is known about the natural history of dispersal in this sys-  
118 tem and the seeds lack rewards to attract animal dispersers. We also used re-surveys  
119 of permanent transects as an independent measure of encroachment that provided a  
120 benchmark against which to evaluate model predictions. The SIPM accounts for size-  
121 structured demography of creosotebush, allows us to test whether shrub expansion is  
122 pulled by the low-density front or pushed from the high-density core, and identifies the  
123 local (demographic) and spatial (seed dispersal) life cycle transitions that most strongly  
124 contribute to expansion speed. We address the following specific questions:

- 125 1. What is the nature of conspecific density dependence in demographic vital rates  
126 along shrub encroachment ecotones? Is encroachment pulled by the individuals at  
127 the front or pushed by individuals behind it?
- 128 2. What is the seed dispersal kernel for this species and how does this vary with  
129 maternal plant size?
- 130 3. What is the predicted rate of expansion and which lower-level processes most  
131 strongly affect the expansion speed?
- 132 4. How does the observed rate of encroachment in the recent past compare to model



133 predictions?

## 134 **Materials and methods**

### 135 *Study species*

136 Creosotebush *Larrea tridentata* is a perennial, drought-resistant shrub that is native to  
137 the arid and semiarid regions of the southwestern United States and northern Mexico.  
138 High-density areas of creosotebush consist largely of barren soil between plants due to  
139 the “islands of fertility” these shrubs create around themselves (Reynolds et al., 1999;  
140 Schlesinger et al., 1996), though lower-density areas will often contain grasses in the  
141 inter-shrub spaces (Fig. 1). In our northern Chihuahuan desert study region creosote-  
142 bush reproduces sexually, with numerous small yellow flowers giving rise to highly  
143 pubescent spherical fruits several millimetres in diameter; these fruits consist of five  
144 carpels, each of which contains a single seed. Seeds are dispersed from the parent plant  
145 by gravity and wind, with the possibility for seeds to subsequently be transported by  
146 animals or water (Maddox and Carlquist, 1985). In other regions, this species also repro-  
147 duces asexually and can give rise to long-lived clonal stands (Vasek, 1980), but this does  
148 not occur in our study region. The foliage is dark green, resinous, and unpalatable to  
149 most grazing and browsing animals (Mabry et al., 1978).

### 150 *Study site*

151 We conducted our work at the Sevilleta National Wildlife Refuge (SNWR), a Long-Term  
152 Ecological Research (SEV-LTER) site in central New Mexico. The refuge exists at the in-  
153 tersection of several eco-regions, including the northern Chihuahuan Desert, Great Plains  
154 grassland, and steppes of the Colorado Plateau. Annual precipitation is approximately

155 250 mm, with the majority falling during the summer monsoon season from June to  
156 September. The recruitment events that facilitate creosotebush expansion are thought to  
157 be episodic (Peters and Yao, 2012), and this may be linked to fluctuations in monsoon  
158 precipitation (Bowers et al., 2004; Boyd and Brum, 1983).

## 159 *Demographic data*

### 160 *Ecotone transects*

161 We collected demographic data during early June of every year from 2013-2017. This  
162 work was conducted at four sites in the eastern part of SNWR (one site was initiated in  
163 2013 and the other three in 2014), with three transects at each site. All transects were  
164 situated along a shrubland-grassland ecotone so that a full range of shrub densities was  
165 captured: each transect spanned core shrub areas, grassland with no or few shrubs,  
166 and the transition between them. Lengths of these transects varied from 200 to 600 m,  
167 determined by the strength of vegetation transition since “steep” transitions required  
168 less length to capture the full range of shrub density.

169 We quantified shrub density in 5-meter “windows” along each transect, including all  
170 shrubs within one meter of the transect on either side (shrubs that partially overlapped  
171 with the census area were included). Densities were quantified once for each transect  
172 (in 2013 or 2014) and were assumed to remain constant for the duration of the study, a  
173 reasonable assumption for a species with very low recruitment and very high survival  
174 of established plants. Given the population’s size structure, we weighted the density of  
175 each window by the sizes of the plants, which we quantified as volume ( $\text{cm}^3$ ). Volume  
176 was calculated as that of an elliptic cone:  $V_i = \frac{\pi h}{3} \frac{lw}{4}$  where  $l$ ,  $w$ , and  $h$  are the max-  
177 imum length, maximum width, and height, respectively. Maximum length and width  
178 were measured so that they were always perpendicular to each other, and height was

179 measured from the base of the woody stem at the soil surface to the tallest part of the  
180 shrub. The weighted density for a window was then expressed as  $\log(\text{volume})$  summed  
181 over all plants in the window.

## 182 *Observational census*

183 At approximately 50-m intervals along each transect we tagged up to 10 plants for annual  
184 demographic census and recorded their local (5-m resolution) window so that we could  
185 connect individual demographic performance to local density. These tagged shrubs were  
186 revisited every June and censused for survival (alive/dead), size (width, length, and  
187 height, as above), flowering status, and fertility of flowering plants (numbers of flower-  
188 buds, flowers, and fruits). In instances where shrubs had large numbers of reproductive  
189 structures that would be difficult to reliably count (a large shrub may have thousands of  
190 flowers or fruits), we made counts on a fraction of the shrub and extrapolated to esti-  
191 mate whole-plant reproduction. Creosotebush does not have one discrete reproductive  
192 event per year; instead, flowering may occur throughout much of the warm season. By  
193 combining counts of buds, flowers, and fruits we intended to capture a majority of the  
194 season's reproductive output, assuming that all buds and flowers will eventually become  
195 fruits. Our measurements of reproductive output are therefore conservative and may un-  
196 derestimate total seed production for an entire transition year. Each year, we searched  
197 for new recruits within one  $m$  on either side of the transect. New recruits were tagged  
198 and added to the demographic census. The observational census included a total of 522  
199 unique individuals.

## 200 *Transplant experiment*

201 We conducted a transplant experiment in 2015 to test how shrub density affects seedling  
202 survival. This approach complemented observational estimates of density dependence  
203 and filled in gaps for a part of the shrub life cycle that was rarely observed due to low  
204 recruitment. Seeds for the experiment were collected from plants in our study popu-  
205 lation in 2014. Seeds were germinated on Pro-Mix potting soil (Quakertown, PA) in  
206 Fall 2014 and seedlings were transferred to 3.8 cm-by-12.7 cm cylindrical containers and  
207 maintained in a greenhouse at Rice University. Seedlings were transported to SNWR  
208 and transplanted into the experiment during July 27-31, 2015. Transplant timing was  
209 intended to coincide with the monsoon season, when most natural recruitment occurs.

210 The transplant experiment was conducted at the same four sites and three transects  
211 per site as the observational demographic census, where we knew weight shrub densities  
212 at 5-m window resolution. We established 12 1-m by 1-m plots along each transect. Plots  
213 were intentionally placed to capture density variation: four plots were in windows with  
214 zero shrubs, four plots were placed in the top four highest-density windows on the  
215 transect, and the remaining four plots were randomly distributed among the remaining  
216 windows with weighted density greater than zero. Plots were placed in the middle of  
217 each 5-m window (at meter 2.5) and were divided into four 0.5-m by 0.5-m subplots.  
218 We divided each subplot into nine squares (0.125-m by 0.125-m) and recorded ground  
219 cover of each square as one of the following categories: bare ground, creosotebush,  
220 black grama (*B. eriopoda*), blue grama (*B. gracilis*), other grass, or “other”. Each subplot  
221 received one transplanted shrub seedling, for a total of 48 transplants per transect, 144  
222 transplants per site, and 576 transplants in the entire experiment. Each site was set  
223 up on a different day and there was a significant monsoon event after the third and  
224 before the fourth site. This resulted in differential mortality that appears to be related

225 to site (captured as a statistical random effect) but more likely reflects the timing of the  
226 monsoon event relative to planting (moist soil likely promoted transplant survival). We  
227 revisited the transplant experiment on October 24, 2015 to survey mortality. After that  
228 first visit, transplants were censused along with the naturally occurring plants each June,  
229 following the methods described above.

### 230 *Demographic analysis*

231 We fit statistical models to the demographic data and used AIC-based model selection to  
232 evaluate empirical support for alternative candidate models. The top statistical models  
233 were then used as the vital rate sub-models of the SIPM, so there is a strong connection  
234 between the statistical and population modeling, as is typical of integral projection mod-  
235 eling. Our analyses focused on the following demographic vital rates: survival, growth,  
236 probability of flowering, fertility (flower and fruit production), seedling recruitment, and  
237 seedling size. Most of these vital rates were modeled as a function of plant size, and all  
238 of them included the possibility of density dependence.

239 The alternative hypotheses of pushed versus pulled wave expansion rest on how the  
240 rate of population increase ( $\lambda$ ), derived from the combination of all vital rates, respond  
241 to density. We were particularly interested in whether demographic performance was  
242 maximized as local density goes to zero (pulled) or at non-zero densities behind the  
243 wave front (pushed). To flexibly model density dependence and detect non-monotonic  
244 responses, we used generalized additive models in the R package ‘mgcv’ (Wood, 2017).  
245 For each vital rate, we fit candidate models with or without a smooth term for local  
246 weighted density (among other possible covariates). To avoid over-fitting, we set the  
247 ‘gamma’ argument of gam() to 1.8, which increases the complexity penalty, results in  
248 smoother fits (Wood, 2017), and makes our approach more conservative (other gamma

249 values yielded qualitatively similar results). We pooled data across transition years for  
250 analysis. All models included the random effect of transect (12 transects across 4 sites);  
251 we did not attempt to model both site and transect-within-site random effects due to the  
252 low numbers of each. All vital rate functions used the natural logarithm of volume ( $\text{cm}^3$ )  
253 as the size variable and the sum of  $\log(\text{volume})$  as the weighted density of a transect  
254 window.

255 *Survival.* We modeled survival or mortality in year  $t + 1$  as a Bernoulli random variable  
256 with three candidate models for survival probability. These included smooth terms for  
257 initial size in year  $t$  only (1), initial size and weighted density (2), and both smooth terms  
258 plus an interaction between initial size and weighted density (3). We analyzed survival of  
259 experimental transplants and observational census plants together in the same analyses,  
260 with a fixed effect of transplant status (yes/no) included in all candidate models. Since  
261 recruits and thus mortality events were both very rare in the observational survey, this  
262 approach allowed us to “borrow strength” over both data sets to generate a predictive  
263 function for size- and possibly density-dependent survival while statistically accounting  
264 for differences between experimental and naturally occurring plants. Because we had  
265 additional, finer-grained cover data for the transplant experiment that we did not have  
266 for the observational census, we conducted an additional stand-alone analysis of trans-  
267 plant survival that explored the influence of shrub and grass density at multiple spatial  
268 scales (Appendix).

269 *Growth.* We modeled size in year  $t + 1$  as a Gaussian random variable. There were nine  
270 candidate models for growth. The simplest model (1) defined the mean of size in year  
271  $t + 1$  as a smooth function of size in year  $t$  and constant variance. Models (2) and (3)  
272 had constant variance but the mean included smooth terms for initial size and weighted

273 density (2) or both smooth terms plus an interaction between initial size and weighted  
274 density (3). Models 4-6 had the same mean structure as 1-3 but defined the standard  
275 deviation of size in year  $t + 1$  as a smooth function of initial size. Models 7-9 mirrored 4-6  
276 and additionally included a smooth term for weighted density in the standard deviation.  
277 Modeling growth correctly is important because it defines the probability of any future  
278 size conditional on current size, a critical element of the IPM transition kernel. We  
279 verified that the AIC-selected model described the data well by simulating data from it  
280 and comparing the moments (mean, variance, skewness, and kurtosis) of simulated and  
281 real data.

282 *Flowering and fruit production.* We modeled shrub reproductive status (vegetative or  
283 flowering) in year  $t$  as a Bernoulli random variable with three candidate models for  
284 flowering probability. These included smooth terms for current size (in year  $t$ ) only (1),  
285 size and weighted density (3), and both smooth terms plus an interaction between size  
286 and weighted density. We modeled the reproductive output of flowering plants (the sum  
287 of flowerbuds, open flowers, and fruits) in year  $t$  as a negative binomial random variable.  
288 There were three candidate models for mean reproductive output that corresponded to  
289 the same three candidates for flowering probability.

290 *Recruitment and recruit size.* We modeled seedling recruitment in each transect window  
291 as a binomial random variable given the number of total seeds produced in that window  
292 in the preceding year. There were two candidate models, with and without an influence  
293 of weighted density on the per-seed recruitment probability. To estimate window-level  
294 seed production, we used the best-fit models for flowering and fruit production and  
295 applied this to all plants in each window that we observed in our initial density surveys.  
296 We assume that recruits come from the previous year's seeds and not from a long-lived

297 soil seed bank.

298 We modeled recruit size as a Gaussian-distributed random variable and fit four can-  
299 didate models including an influence of weighted density on mean, variance, both, and  
300 neither.

### 301 *Density-dependent IPM*

302 The size- and density-dependent statistical models comprised the sub-models of a den-  
303 sity dependent Integral Projection Model (IPM) that we used to evaluate how the shrub  
304 population growth rate responded to con-specific density; we present this non-spatial  
305 model before layering on the spatial dynamics generated by seed dispersal. A basic  
306 density-independent IPM predicts the number of individuals of size  $x'$  at time  $t + 1$   
307 ( $n(x', t + 1)$ ) based on a demographic projection kernel ( $K_{dem}$ ) that gives the rates of tran-  
308 sition from sizes  $x$  to  $x'$  from times  $t$  to  $t + 1$  and is integrated over the size distribution  
309 from the minimum ( $L$ ) to maximum ( $U$ ) sizes. In a density-dependent IPM, components  
310 of the projection kernel may respond to population abundance and structure:

$$311 \quad n(x', t + 1) = \int_L^U K_{dem}(x', x, \tilde{n}(t)) n(x, t) dx \quad (1)$$

312 Here,  $\tilde{n}(t)$  is some function of population structure  $n(x, t)$  such as the total density of  
313 conspecifics ( $\tilde{n}(t) = \int n(x, t) dx$ ) or, as in our case, total density weighted by size ( $\tilde{n}(t) =$   
314  $\int x n(x, t) dx$ ). For simplicity, in the analyses that follow we do not model density as  
315 a dynamic state variable; instead, we treat density as a static covariate ( $\tilde{n}(t) = \tilde{n}$ ) and  
316 evaluate the IPM at a range of density values. As in our statistical modeling, the size  
317 variable of the IPM ( $x, x'$ ) was  $\log(cm^3)$ .

318 For our model, the size- and density-dependent demographic transitions captured by  
319 the projection kernel include growth or shrinkage ( $g$ ) from size  $x$  to  $x'$  conditioned on



survival ( $s$ ) at size  $x$  (combined growth-survival function  $G(x', x, \tilde{n}) = g(x', x, \tilde{n})s(x, \tilde{n})$ ),  
 and the production of new size- $x'$  individuals from size- $x$  parents ( $Q(x', x, \tilde{n})$ ). Repro-  
 duction reflects the probability of flowering at size  $x$  ( $p$ ), the number of seeds produced  
 by flowering plants ( $d$ ), the per-seed probability of recruitment ( $r$ ), and the size distribu-  
 tion of recruits ( $c$ ). Collectively, the rate at which  $x$ -sized individuals produce  $x'$ -sized  
 individuals at density  $\tilde{n}$  is given by the combined reproduction-recruitment function  
 $Q(x', x, \tilde{n}) = p(x, \tilde{n})d(x, \tilde{n})r(\tilde{n})c(x', \tilde{n})$ . Thus, we can express the projection kernel as:

$$K_{dem}(x', x, \tilde{n}) = G(x', x, \tilde{n}) + Q(x', x, \tilde{n}) \quad (2)$$

For analysis, we evaluated the IPM kernel over a range of local densities from the mini-  
 mum to the maximum of weighted density values from the 5-meter windows ( $0 \leq \tilde{n} \leq$   
 $\tilde{n}_{max}$ ). At each density level, we discretized the IPM kernel into a  $200 \times 200$  approxim-  
 ating matrix and calculated the asymptotic growth rate  $\lambda(\tilde{n})$  as its leading eigenvalue. We  
 extended the lower ( $L$ ) and upper ( $U$ ) integration limits to avoid unintentional “eviction”  
 using the floor-and-ceiling method (Williams et al., 2012).

We sought to characterize the shape of density dependence: whether fitness declined  
 monotonically or not with increasing density. We quantified uncertainty in the density-  
 dependent growth rate  $\lambda(\tilde{n})$  by bootstrapping our data. For each bootstrap, we ran-  
 domly sampled 75% of our demographic data, re-ran the statistical modeling and model  
 selection, and used the top vital rate models to generate  $\lambda(\tilde{n})$  for that data subset. We  
 repeated this procedure for 500 bootstrap replicates.

## Dispersal modelling

*WALD dispersal model.* Dispersal kernels were calculated using the WALD, or Wald analytical long-distance dispersal, model that uses a mechanistic approach to predict dispersal patterns of plant propagules by wind. The WALD model, which is based in fluid dynamics, can serve as a good approximation of empirically-determined dispersal kernels (Katul et al., 2005; Skarpaas and Shea, 2007) and may be used when direct observations of dispersal are not available. Under the assumptions that wind turbulence is low, wind flow is vertically homogenous, and terminal velocity is achieved immediately upon seed release, the WALD model simplifies a Lagrangian stochastic model to create a dispersal kernel that estimates the likelihood a propagule will travel a given distance (Katul et al., 2005). Our dispersal kernel takes the form of the inverse Gaussian distribution, using  $r$  to denote dispersal distance:

$$p(r) = \left( \frac{\lambda'}{2\pi r^3} \right)^{\frac{1}{2}} \exp \left[ -\frac{\lambda'(r - \mu')^2}{2\mu'^2 r} \right] \quad (3)$$

Here,  $\lambda'$  is the location parameter and  $\mu'$  is the scale parameter, which depend on environmental and plant-specific properties of the study system. (We use  $\lambda'$  for consistency with notation in related papers, but  $\lambda'$  the dispersal location parameter should not be confused with  $\lambda$  the geometric growth rate.) The location and scale parameters are defined as  $\lambda' = (H/\sigma)^2$  and  $\mu' = HU/F$ ; these are functions of the height  $H$  of seed release, wind speed  $U$  at seed release height, seed terminal velocity  $F$ , and the turbulent flow parameter  $\sigma$  that depends on both wind speed and local vegetation roughness. We parameterized the WALD dispersal kernel using windspeed data from the SEV-LTER weather station nearest our study site (Moore and Hall, 2022) and seed terminal velocity data from laboratory-based seed-drop experiments (Appendix A). We integrated the dis-

persal kernel over observed variation in wind speeds, seed terminal velocity, and release height within the height of a shrub. Therefore the dispersal kernel for a shrub of height  $U$  was given by:

$$K_{disp} = \iiint p(F)p(U)p(z)p(r) dF dU dz \quad (4)$$

and  $p(F)$  and  $p(U)$  are the PDFs of the terminal velocity  $F$  and wind speed  $U$ , respectively, and  $p(z)$  is the uniform distribution from the minimum seed release height ( $0.15m$ , the height at which grass cover interferes with wind dispersal) to  $H$ . Methods for our seed data collection and technical details of dispersal kernel modeling are provided in Appendix A.

### *Spatial integral projection model*

We used a spatial integral projection model to piece together seed dispersal and density-dependent demography, and generate predictions for the rate of shrub expansion that results from this combination of local and spatial processes. The spatially explicit model builds upon the non-spatial model (Eq. 1) and adds a spatial variable ( $z, z'$ ) such that demographic transitions occur across both time and space according to a combined demography-dispersal kernel  $\tilde{K}$ :

$$n(x', z', t + 1) = \int_{-\infty}^{+\infty} \int_L^U \tilde{K}(x', x, z', z, \tilde{n}(z, t)) n(x, z, t) dx dz \quad (5)$$

Here,  $\tilde{K}(x', x, z', z, \tilde{n}(z, t))$  describes the transition from size  $x$  and location  $z$  to size  $x'$  and location  $z'$  given density  $\tilde{n}(z, t)$  at starting location  $z$ . As before,  $\tilde{n}$  is a function of population structure – in our model, weighted local density – but here integrated over an explicit competitive “neighborhood”:  $\tilde{n}(z, t) = \int_{z-h}^{z+h} \int_L^U x n(x, z, t) dx dz$  where  $h$

384 represents neighborhood size in the units of  $z$ . The demography-dispersal kernel  $\tilde{K}$  is  
 385 given by the sum of two parts, one that describes reproduction coupled with dispersal of  
 386 propagules, and another that describes growth and survival of non-dispersing individu-  
 387 als:

$$388 \quad \tilde{K}(x', x, z', z, \tilde{n}(z, t)) = K_{disp}(z' - z)Q(x', x, \tilde{n}) + \delta(z' - z)G(x', x, \tilde{n}) \quad (6)$$

389 Here, regeneration function  $Q$  and growth-survival function  $G$  correspond to Eq. 2,  
 390 dispersal kernel  $K_{disp}$  corresponds to Eq. , and the Dirac delta function is a probability  
 391 distribution with all mass at zero, which prevents movement during survival and size  
 392 transition. Following standard assumptions for integro-difference equations, we assume  
 393 that space is one-dimensional and homogeneous, such that demographic transitions do  
 394 not depend on location (or, more precisely, that they depend on location only through  
 395 spatial variation in density) and the probability of dispersing from location  $z$  to  $z'$  de-  
 396 pends only on the absolute distance between them.

397 Under many conditions, models of this form generate traveling waves, and we are  
 398 particularly interested in the velocity ( $m/yr$ ) of this wave. Methods to estimate this ve-  
 399 locity depend strongly on how demography responds to density. If fitness is maximized  
 400 at some density  $\tilde{n} > 0$  then the wave is pushed and wave velocity can only be estimated  
 401 through numerical simulation. However, if fitness is maximized at  $\tilde{n} = 0$  then the wave  
 402 is pulled and an upper bound on its asymptotic velocity can be calculated analytically,  
 403 following Neubert and Caswell (2000) and Jongejans et al. (2011), as

$$404 \quad c^* = \min_{s>0} \left[ \frac{1}{s} \ln(\rho_s) \right] \quad (7)$$

405 where  $s$  is a wave shape parameter and  $\rho_s$  is the dominant eigenvalue of the kernel

406  $H_s(x', x)$ . Corresponding to Eq. 6 and assuming  $\tilde{n} = 0$ ,  $H_s$  is composed of

$$407 \quad H_s(x', x) = M(s, x)Q(x', x) + G(x', x) \quad (8)$$

408 where  $M(s, x)$  is the moment-generating function (MGF) for the dispersal kernel as-  
409 sociated with size  $x$ . This formulation of the model assumes that the dispersal kernel  
410 depends only on maternal size  $x$  and not offspring size  $x'$ . To estimate  $M(s, x)$  we sim-  
411 ulated  $N = 10000$  dispersal events ( $r$ ) for each size  $x$  and marginalized these over one  
412 spatial dimension as in Lewis et al. (2006). We then evaluated the empirical MGF for  
413 each size  $x$ :  $M(s) = \frac{1}{N} \sum_{i=1}^N e^{sr}$ .

414 We used numerical sensitivity analysis to compare the contributions of demography  
415 and dispersal processes to the speed of expansion. We perturbed each vital rate function  
416 by an arbitrary value, recalculated wavespeed, and quantified sensitivity as the change  
417 in wavespeed divided by the perturbation. Analytical sensitivity analysis is also possible  
418 (Ellner et al., 2016) but these sensitivities reflect infinitesimally small perturbations. We  
419 were particularly interested in the effects of large perturbations, especially large changes  
420 in seedling recruitment, which is subject to pulse events.

421 Estimates of wavespeed and its sensitivity to demography and dispersal processes  
422 were bootstrapped for a total of 1000 replicates. Each bootstrap replicate recreated size-  
423 and density-dependent demographic models using 50% resampling on the original de-  
424 mographic data, and recreated dispersal kernels also using 50% resampling on the wind  
425 speeds and seed terminal velocities. Model selection for demographic vital rates was re-  
426 run for each bootstrap replicate. The empirical MGF relied on numerical sampling and  
427 was therefore sensitive to extreme long-distance events that differed across bootstrap  
428 realizations. Therefore, bootstrapped distributions reflect the combination of model un-  
429 certainty, parameter uncertainty, and stochasticity inherent to empirical MGFs.

## *Encroachment re-surveys*

Finally, we used re-survey data from permanent transects to assess the predictions of the SIPM with respect to independent empirical observations. In summer 2001, shrub percent cover was recorded along two permanent 1000-m transects that spanned the shrub-grass ecotone (these were different transects than those described above for shrub demography). Surveys were conducted again in summer 2013 to document change in creosotebush abundance and spatial extent. At every 10 meters, shrub cover was recorded in nine cover classes (<1%, 1–4%, 5–10%, 10–25%, 25–33%, 33–50%, 50–75%, 75–95%, >95%). For visualization, we show midpoint values of these cover classes at each meter location for both transects and years.

## **Results**

### *Size and density dependent demography*

Demographic data from naturally occurring and transplanted individuals revealed strong size- and density-dependence in demographic vital rates. For most sizes and vital rates, shrub density had negative demographic effects; there was no strong evidence for positive density dependence in any demographic process at any size. Statistical support for size- and density-dependence is provided in Tables B1–B6, which provide AIC rankings for candidate models based on the complete data set.

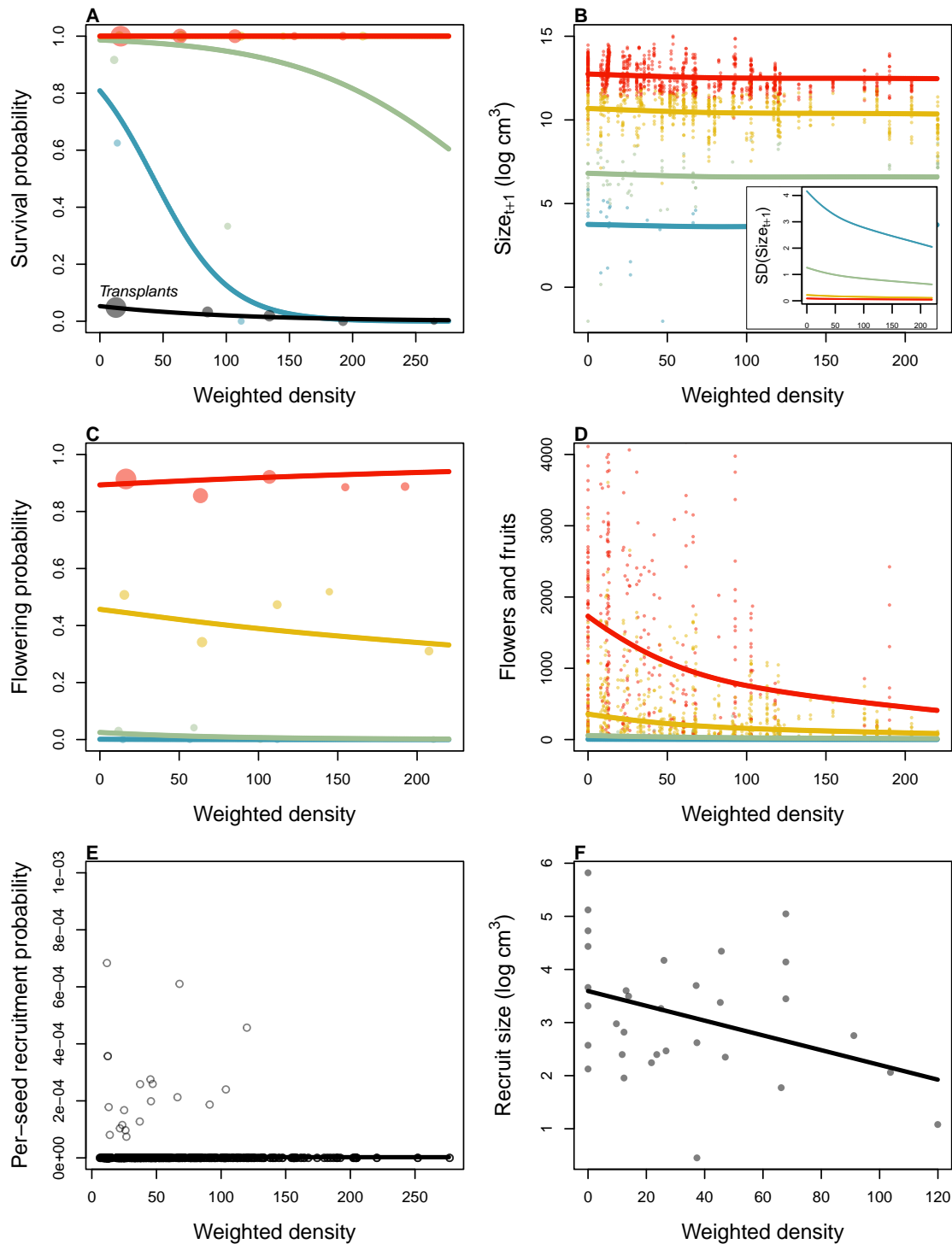


Figure 2: Size- and density-dependence in demographic vital rates. **A** Probability of survival from natural population census and transplant experiment (black line), **B** Mean and variance (inset) of size conditional on previous size, **C** Probability of flowering, **D** Flower and fruit production, **E** Probability of recruitment per seed, **F** Recruit size. In **A**–**E**, colored lines indicate four size groups (red is largest, blue is smallest), discretized for data visualization only. In all panels, weighted density is the sum of all plant sizes  $\log(\text{cm}^3)$  within the same 5-m window as the census individual.

448 *Survival.* Among naturally occurring plants, survival of large, established individuals  
449 was very high (Fig. 2A). We observed relatively few mortality events and nearly all of  
450 these were among new recruits. The probability of survival at these small sizes declined  
451 with increasing density. Survival of transplants was very low, lower even than survival  
452 of similarly-sized, naturally occurring recruits (Fig. 2B). However, the transplant results  
453 support the general pattern of negative density dependence in survival. Among the  
454 20 survivors, 15 of them occurred in transect windows below the median of weighted  
455 shrub density. In Appendix B, we show that transplant mortality was dominated by  
456 negative effects of shrub density at the 5-m window scale, even when effects of local  
457 grass and shrub cover were included as alternative or additional statistical covariates,  
458 which suggests that this is the appropriate spatial scale for modeling density dependence  
459 in this system.

460 *Growth.* Current size was strongly predictive of future size, as expected, and there was  
461 weak negative density dependence in mean future size conditioned on current size (Fig.  
462 2C). However, there was a stronger signal of density dependence in the variance of fu-  
463 ture size (Fig. 2C, inset). Plants at low density exhibited greater variance in growth  
464 trajectories and this was especially true at the smallest sizes. Thus, large increases (and  
465 decreases) in the size of new recruits were most likely to occur under low-density condi-  
466 tions.

467 *Flowering and fruit production.* Flowering probability was strongly size-dependent and  
468 and very weakly sensitive to local density (Fig. 2D). However, fertility of flowering plants  
469 was strongly negative density dependent, with greatest flower and fruit production by  
470 the largest plants at the lowest densities, and vice versa (Fig. 2E).



471 *Recruitment and recruit size.* We observed 32 natural recruitment events along our tran-  
472 sects during the study years and our estimate recruitment rate, given total expected seed  
473 production in each window preceding the recruitment year, was very low ( $2.47 \times 10^{-6}$ ,  
474 2E). While most recruitment events occurred at low density, this is also where most seed  
475 production was concentrated (Fig. 2E) and low-density windows were over-represented  
476 relative to high density. For these reasons we were more likely to observe recruitment  
477 events at low density. Controlling for sampling effort and seed production, the sta-  
478 tistical models indicated that our data were most consistent with a constant, density-  
479 independent seed-to-seedling recruitment rate (Table B5). However, the mean size of  
480 new recruits declined significantly with local density (Fig. 2F).

481 *Population growth rate.* As expected given the vital rate results, the asymptotic popula-  
482 tion growth rate  $\lambda$  declined monotonically with density (Fig. 3). This was true across  
483  $> 98\%$  of bootstrap replicates, indicating high certainty that shrub fitness is maximized at  
484 zero density and thus that the expansion wave is “pulled” (for this reason our wavespeed  
485 results are based on the analytical approach described above). Mean growth rate at low  
486 density was 3% per year, with bootstrap uncertainty spanning 1–6%. At high density in  
487 the core of the expansion wave, population growth rates approached  $\lambda = 1$ , indicating  
488 population stasis driven by near-immortality and extremely rare recruitment.

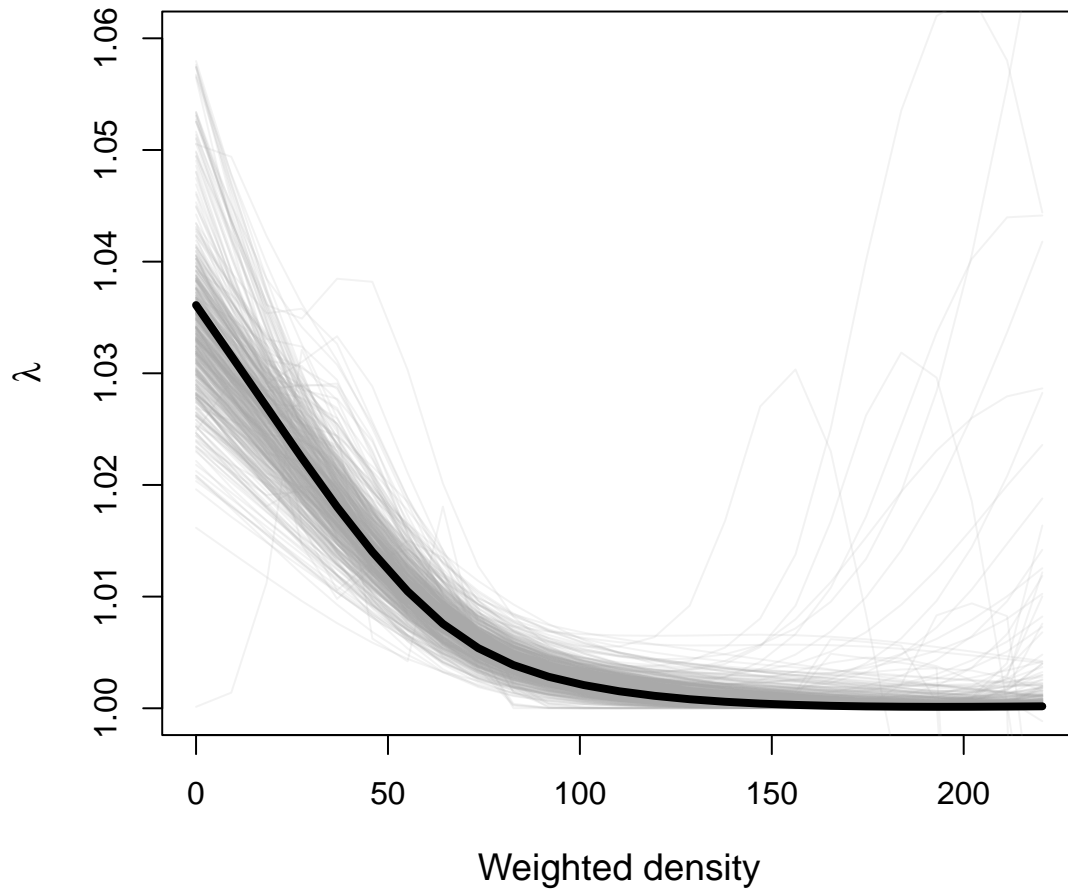


Figure 3: Density dependence in the asymptotic population growth rate ( $\lambda$ ). Lines show bootstrap replicates sub-sampled from the full demographic data set. Weighted deighted density is the sum of all plant sizes  $\log(\text{cm}^3)$  within 5-m windows.

### *Seed dispersal*

489

490 WALD dispersal kernels were inferred from the properties of seeds and wind and ac-  
 491 counted for observed variation in wind speeds and within-plant seed release height. The  
 492 resulting kernels were predicted to be strongly size dependent, with taller plants having

493 a greater probability of dispersing seeds longer distances (Fig. 4). However, predicted  
494 seed dispersal was highly local, with most seeds expected to fall within one meter of  
495 parent plants for most sizes. Even for the very tallest shrub we observed (1.96 m), only  
496 6.2% of its seeds were predicted to fall more than 3 m away and less than 1% were pre-  
497 dicted to fall more than 6 m away (Fig. 4). Taller shrubs also exhibited wider variance  
498 in their dispersal kernel and this reflects their wider range of within-shrub seed release  
499 heights.

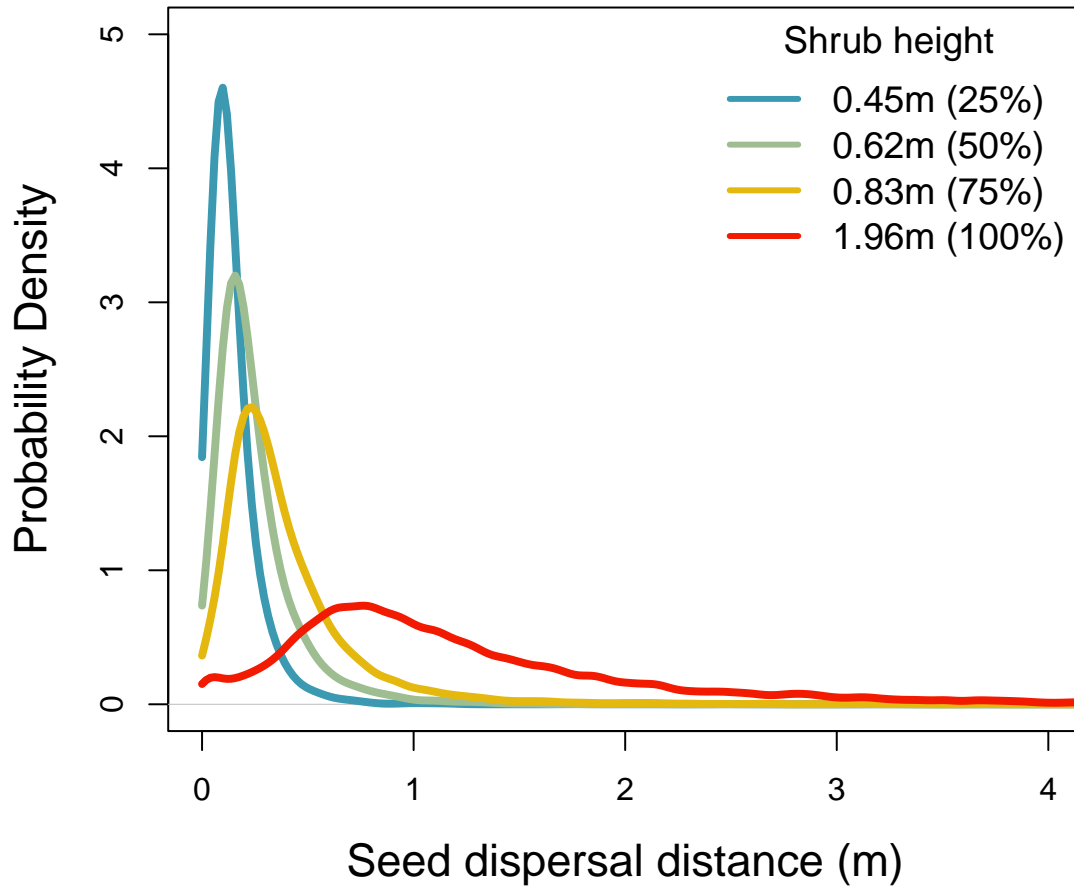


Figure 4: Predicted WALD dispersal kernels for four shrub heights corresponding to the 25th, 50th, 75th, and 100th (maximum) percentiles of the observed size distribution. We assume that heights below 15 cm have effectively no seed movement due to interference with the grass layer.

### *Expansion speed and sensitivities*

The asymptotic speed of creosote encroachment, given the above demography and dispersal patterns, was very slow. The mean asymptotic speed was 0.08 m/year and the 5–95 percentiles of the uncertainty distribution was 0.06–0.12 m/year (Fig. 6A). The

504 sensitivities of wavespeed spanned orders of magnitude, indicating strong inequality  
 505 in the relative importance of the demography and dispersal processes controlling ex-  
 506 pansion (Fig. 6B). Expansion speed was by far the most sensitive to the probability  
 507 of seedling recruitment (Fig. 6B), indicating that this life cycle transition imposes the  
 508 strongest constraint on encroachment. Sensitivity to survival ranked second, and since  
 509 nearly all mortality occurred at the smallest sizes this too can be interpreted as an early  
 510 life cycle constraint on expansion. The mean of growth ranked third and this was also  
 511 likely related to early plant survival, since increases in size allow small plants to reach  
 512 “protected” sizes given the strong size-dependence in survival.

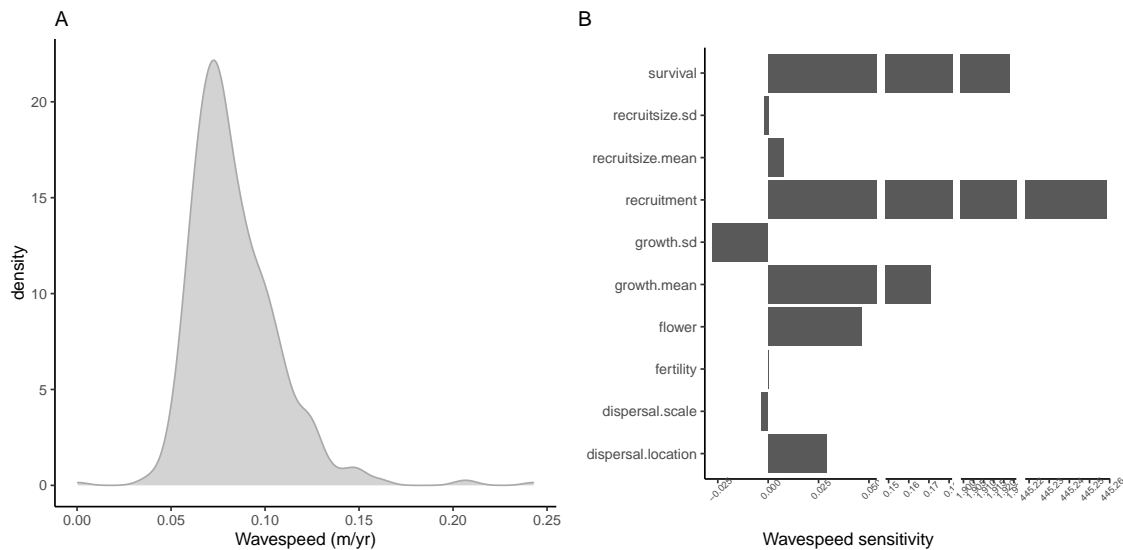


Figure 5: A, Asymptotic speed of creosote encroachment. The distribution reflects parameter and model uncertainties quantified via bootstrapping and stochastic sampling from seed dispersal kernels. B, Sensitivities of wavespeed to demography and dispersal processes. For size-dependent functions (growth, survival, flowering, and fertility) sensitivity was calculated by perturbing the entire function across all sizes.

513

## *Transect re-surveys*

514 Re-surveys along two permanent transects revealed virtually no change the in the cre-  
 515 osote expansion wave over the 12 years that preceded our study. There were local  
 516 changes in percent cover: on average cover increased by XX% between surveys. How-  
 517 ever, there was no clear indication that the leading edge of the creosote shrubland has  
 518 advanced (the modest right-ward shift on both transects is within the range of measure-  
 519 ment error).

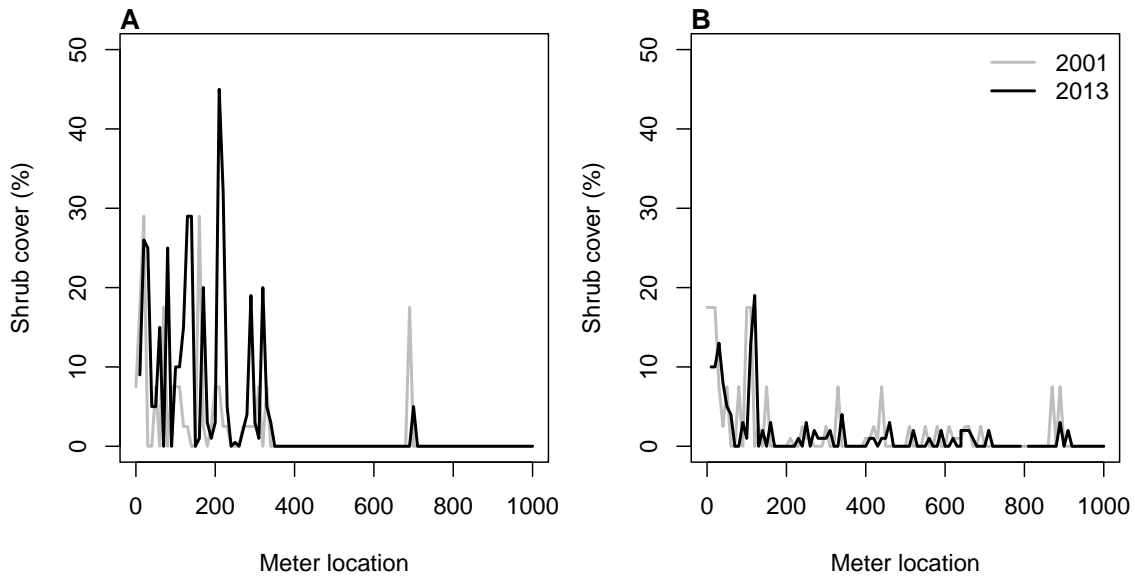


Figure 6: Surveys of creosotebush percent cover along two permanent transects (A,B) in 2001 and 2013.

520

## **Discussion**

521 The encroachment of grasslands by woody plants is a worldwide phenomenon with  
 522 broad implications for biodiversity and ecosystem function. To our knowledge, ours is

523 the first study to apply spatial population biology theory to woody plant encroachment.  
524 This perspective on the problem brings attention to the combined influence of dispersal  
525 and density-dependent demography as critical controls on the occurrence and pace of en-  
526 croachment. Through this lens, we asked whether the encroachment process is pushed or  
527 pulled, hypothesizing that potential for positive feedbacks may cause declines in fitness  
528 at the low-density front and generate pushed-wave dynamics. Instead, observational and  
529 experimental evidence indicate that fitness was maximized in low-density plant neigh-  
530 borhoods. The creosote encroachment wave is therefore predicted to be pulled by maxi-  
531 mum demographic performance at the leading edge. However, our field-parameterized  
532 spatial integral projection model revealed that this wave is pulled at the very slow rate of  
533 6–12 centimeters per year – so slow that, under the observed conditions, this grass-shrub  
534 ecotone is effectively stationary. In fact, to our knowledge, ours is the slowest wavespeed  
535 estimate for a plant population in the demography-dispersal modeling literature (SIPMs  
536 and their matrix model progenitor: (Neubert and Caswell, 2000)). Re-surveys of perma-  
537 nent transects independently supported this prediction, showing virtually no change in  
538 the position of the shrub boundary in over a decade. Whatever historical conditions al-  
539 lowed for shrub encroachment to its current extent, the encroachment wave is presently  
540 stalled. Below, we discuss and interpret these key findings and their broader implications  
541 in greater detail.

542     Observational and experimental evidence strongly indicated that effects of shrub den-  
543 sity were strongly negative in all vital rates and at all sizes. This was surprising given  
544 widespread evidence for positive feedbacks (which should generate low-density fitness  
545 penalties) in woody plant encroachment generally (D’odorico et al., 2013) and specifi-  
546 cally in our creosote bush system (D’Odorico et al., 2010). How can we square these  
547 apparently conflicting results? First, it may be important to consider the distinction be-

548 tween “demographic” and “component” Allee effects (Stephens et al., 1999), which refer  
549 to effects that manifest in total fitness and components of fitness, respectively. That is,  
550 positive effects of conspecific density may occur but in our measures of demographic  
551 performance these are swamped by stronger, counter-acting negative effects. It is worth  
552 noting that our demographic measurements are temporally coarse, reflecting aggregate  
553 performance over a full transition year. More mechanistic studies on finer time scales  
554 might reveal component Allee effects that are masked by strong net-negative density  
555 dependence. Second, many of the potential mechanisms for positive feedbacks at shrub-  
556 grass ecotones would manifest infrequently. For example, effects of shrub encroachment  
557 on microclimate (D’odorico et al., 2013) may promote shrub survival only in the face of  
558 rare climate events such as extreme low temperatures. Similarly, positive feedbacks that  
559 occur via fire suppression (Collins et al., 2021; Ratajczak et al., 2011) would only manifest  
560 on timescales that are inclusive of fire return intervals. These considerations suggest that  
561 we may be more likely to detect positive density dependence over longer time scales  
562 that encompass conditions that trigger positive feedbacks. This leads to the hypothesis  
563 that the shrub encroachment wave is *usually* pulled but occasionally pushed. To our  
564 knowledge such switches have never been empirically documented in any expanding  
565 population but may be an important feature of expansion in fluctuating environments.

566 The very low transplant survival and recruitment rates that we measured also call  
567 attention to time scale. Previous studies suggest that creosote recruitment is strongly  
568 episodic, likely in response to large, infrequent monsoon precipitation events (Allen  
569 et al., 2008; Boyd and Brum, 1983; Moreno-de las Heras et al., 2016). Similar patterns  
570 of episodic recruitment driven by large precipitation events have been observed in other  
571 cases of woody plant encroachment in aridlands (Harrington, 1991; Weber-Grullon et al.,  
572 2022), and relatively high transplant survival on the one transect that we planted im-



573 mediate following a large monsoon event anecdotally supports an important role for  
574 soil moisture. With only four transition-years of demographic data, we chose to com-  
575 bine information across years and build a deterministic model that averages over inter-  
576 annual variability. However, the connection between shrub recruitment and monsoon  
577 precipitation, combined with the observed and projected increase in the variability of  
578 monsoon precipitation in our study region (Petrie et al., 2014), suggest that extending  
579 our deterministic model to accommodate inter-annual variability in climate and climate-  
580 dependent vital rates will be a critical next step. Because our wavespeed estimate is  
581 acutely sensitive to the seed-to-seedling transition, more so than any other demographic  
582 or dispersal process, we expect that a stochastic model incorporating many years of data  
583 may yield a faster predicted expansion speed driven by rare pulses of recruitment (Ell-  
584 ner and Schreiber, 2012). Such pulses have clearly not occurred during our study years  
585 (2013–2017) or the preceding decade of transect re-surveys (2001–2012) and therefore  
586 we think the deterministic model is an adequate representation of the observed condi-  
587 tions. However, our findings of pulled-wave dynamics and strong wavespeed sensitivity  
588 to seedling recruitment indicate that the present shrub ecotone is primed for expansion  
589 once the necessary climate conditions align, as they likely will in a more variable cli-  
590 mate regime. While monsoon precipitation is a leading candidate for factors promoting  
591 seedling establishment, it is worth noting that our study years included both the lowest  
592 and second-highest amounts of monsoon precipitation in a 20-year record, and yet these  
593 events did not correlate with seedling recruitment on our transects (Fig. B1). The condi-  
594 tions favoring recruitment and recruit survival may therefore be more complicated than  
595 the single driver of monsoon precipitation.

596 While not as strong a constraint as recruitment based on our sensitivity analysis,  
597 limited dispersal ability also contributed to the very slow predicted speed of encroach-

ment. Our mechanistic dispersal modeling assumes that wind is the sole dispersal vector. Previous work suggests that this modeling approach can accurately predict dispersal patterns for wind-dispersed plants (Skarpaas and Shea, 2007), yet in our system it may be important to consider secondary dispersal vectors. Boyd and Brum’s 1983 study of creosote bush reproductive biology described “contradiction in the literature about mode of dispersal”, citing evidence for a dominant role of wind but the additional possibility of seed movement by granivorous animals. Combining wind and animal dispersal vectors into a “total” dispersal kernel (Rogers et al., 2019) may be a valuable next step. Second, overland flow of runoff may contribute to secondary seed movement following initial deposition by wind (Thompson et al., 2014). Interestingly, seed movement from overland flow would be most likely following large monsoon events. Therefore the same conditions that promote seedling recruitment may also promote long-distance dispersal, potentially amplifying a pulse of shrub encroachment (Ellner and Schreiber, 2012). Seeds may be blown along the ground following initial deposition, which our model does not account for. The classic WALD dispersal model employed here assumes uniform grass cover, with seeds trapped below the height of this grass canopy. As in aridlands worldwide, our northern Chihuahuan Desert study region is characterized by a high percentage of bare ground, especially in areas of high creosote density (Fig. 1). New approaches are needed to extend mechanistic dispersal modeling to accommodate this feature of aridlands, as others have recognized (Thompson et al., 2014). The potential roles for both biotic and abiotic secondary dispersal vectors makes our dispersal kernel a conservative estimate of seed movement and highlights a need for further study of shrub seed dispersal.

Our model focused on intra-specific density dependence but inter-specific plant-plant interactions may be an important element of shrub encroachment. For example, over-

623 grazing is a hypothesized driver of shrub encroachment due to release from grass com-  
624 petition and reduction of grassland fires (Van Auken, 2000). Our shrub encroachment  
625 model considered only one “side” of the grass-shrub ecotone, assuming that the shrub  
626 population spreads into empty space. Explicit consideration of grass competition or fa-  
627 cilitation may enrich our understanding of shrub expansion or lack thereof in this and  
628 other systems. However, our transplant experiment provided no strong evidence for an  
629 influence of grass cover on seedling survival (Appendix B). Similarly, grass competition  
630 had no effect on germination and survival of mesquite (*Prosopis glandulosa*) shrubs in Chi-  
631 huahuan Desert grassland (Weber-Grullon et al., 2022). While our current data do not  
632 allow us to quantify whether and how strongly resident grasses may slow down shrub  
633 encroachment, we can infer that competitive effects of grasses on shrubs are weaker than  
634 competitive effects of shrubs on shrubs. Therefore our conclusion that the encroachment  
635 wave is pulled implicitly accounts for any effects of grass cover.

636 While our data reveal strong negative density dependence, we know little about the  
637 underlying mechanisms that give rise to this pattern. What is it about high shrub density  
638 environments that suppress survival and reproduction? The abundance of bare ground  
639 in core shrubland suggests that shrubs do not compete for space. However, Brisson  
640 and Reynolds (1994) found strong competition for space belowground, with crowded  
641 neighborhoods constraining creosote root systems. Also, root development of creosote  
642 seedlings can respond rapidly to the availability of soil moisture (Obrist and Arnone Iii,  
643 2003), suggesting that competition for water may be another element of density depen-  
644 dence. Finally, negative density dependence in plants may also be mediated by con-  
645 sumers or soil microbes. Better understanding the environmental drivers of density  
646 dependence will enable better prediction for how the encroachment wave may respond  
647 to future environmental change.

648 *Conclusions.* Understanding and predicting the dynamics of woody-herbaceous eco-  
649 tones requires that we build knowledge of the fates of the rare individuals that disperse  
650 from core habitat and cross habitat boundaries. For a creosote bush, there is no better  
651 place to be than alone in a grassland, and that key result governs the spatial dynamics of  
652 this population. We found that wave of creosote bush expansion into Chihuahuan desert  
653 grassland is pulled by peak fitness at the leading edge. However, it is pulled so slowly  
654 that it is effectively stalled, a model-derived prediction that is supported by independent  
655 data. Had we only relied on the re-survey data without insight from the mechanistic  
656 model we might have concluded that the creosote ecotone is stable at its current bound-  
657 ary. Instead, acute sensitivity of a slow wave to seedling recruitment leaves this system  
658 poised for pulses of expansion under the right conditions; what exactly those conditions  
659 is not yet fully resolved. We suggest that the concepts and tools of spatial population biol-  
660 ogy may facilitate advances in the study and management of woody plant encroachment,  
661 which, like all spreading populations, must be driven by birth, death, and movement.

## 662 **Acknowledgements**

663 This research was supported by the Sevilleta LTER program (NSF DEB awards 1655499,  
664 1748133). We are grateful to Andrew Bibian, Aldo Compagnoni, Kevin Czachura, Mar-  
665 ion Donald, Kory Kolis, Johanna Ohm, Rande Patterson, Erendira Quintana Morales,  
666 Olivia Ragni, Emily Schultz, and Charlene Thomas for their contributions to field data  
667 collection. Kat Shea and Olav Skarpaas provided helpful guidance on dispersal model-  
668 ing.<sup>2</sup> This research was permitted by the US Fish and Wildlife Service with a Special Use  
669 Permit.

---

<sup>2</sup>*Correct, Trevor?*

## Author contributions

All authors contributed to study design. THD and TEXM led data analysis, modeling, and writing early drafts of the manuscript. All authors participated in preparing the manuscript for submission.

## Data accessibility

All of our data and code are available during peer review at <https://github.com/TrevorHD/LTEncroachment>.

## Literature Cited

Allen, A., W. Pockman, C. Restrepo, and B. Milne. 2008. Allometry, growth and population regulation of the desert shrub *Larrea tridentata*. *Functional Ecology* pages 197–204.

Bowers, J. E., R. M. Turner, and T. L. Burgess. 2004. Temporal and spatial patterns in emergence and early survival of perennial plants in the Sonoran Desert. *Plant Ecology* **172**:107–119.

Boyd, R. S., and G. D. Brum. 1983. Postdispersal reproductive biology of a Mojave Desert population of *Larrea tridentata* (Zygophyllaceae). *American Midland Naturalist* pages 25–36.

Brandt, J. S., M. A. Haynes, T. Kuemmerle, D. M. Waller, and V. C. Radeloff. 2013. Regime shift on the roof of the world: Alpine meadows converting to shrublands in the southern Himalayas. *Biological Conservation* **158**:116–127.

- 690 Brisson, J., and J. F. Reynolds. 1994. The effect of neighbors on root distribution in a  
691 creosotebush (*Larrea tridentata*) population. *Ecology* **75**:1693–1702.
- 692 Buffington, L. C., and C. H. Herbel. 1965. Vegetational changes on a semidesert grassland  
693 range from 1858 to 1963. *Ecological monographs* **35**:139–164.
- 694 Bullock, J. M., S. M. White, C. Prudhomme, C. Tansey, R. Perea, and D. A. Hooftman.  
695 2012. Modelling spread of British wind-dispersed plants under future wind speeds in  
696 a changing climate. *Journal of Ecology* **100**:104–115.
- 697 Cabral, A., J. De Miguel, A. Rescia, M. Schmitz, and F. Pineda. 2003. Shrub encroachment  
698 in Argentinean savannas. *Journal of Vegetation Science* **14**:145–152.
- 699 Collins, S. L., J. B. Nippert, J. M. Blair, J. M. Briggs, P. Blackmore, and Z. Ratajczak.  
700 2021. Fire frequency, state change and hysteresis in tallgrass prairie. *Ecology Letters*  
701 **24**:636–647.
- 702 D’Odorico, P., J. D. Fuentes, W. T. Pockman, S. L. Collins, Y. He, J. S. Medeiros,  
703 S. DeWekker, and M. E. Litvak. 2010. Positive feedback between microclimate and  
704 shrub encroachment in the northern Chihuahuan desert. *Ecosphere* **1**:1–11.
- 705 D’odorico, P., Y. He, S. Collins, S. F. De Wekker, V. Engel, and J. D. Fuentes. 2013.  
706 Vegetation–microclimate feedbacks in woodland–grassland ecotones. *Global Ecology*  
707 *and Biogeography* **22**:364–379.
- 708 D’Odorico, P., G. S. Okin, and B. T. Bestelmeyer. 2012. A synthetic review of feedbacks  
709 and drivers of shrub encroachment in arid grasslands. *Ecohydrology* **5**:520–530.
- 710 Ellner, S. P., D. Z. Childs, M. Rees, et al. 2016. Data-driven modelling of structured  
711 populations. *A practical guide to the Integral Projection Model*. Cham: Springer .

- 712 Ellner, S. P., and S. J. Schreiber. 2012. Temporally variable dispersal and demography can  
713 accelerate the spread of invading species. *Theoretical Population Biology* **82**:283–298.
- 714 Gandhi, S. R., E. A. Yurtsev, K. S. Korolev, and J. Gore. 2016. Range expansions transition  
715 from pulled to pushed waves as growth becomes more cooperative in an experimental  
716 microbial population. *Proceedings of the National Academy of Sciences* **113**:6922–6927.
- 717 Gardner, J. L. 1951. Vegetation of the creosotebush area of the Rio Grande Valley in New  
718 Mexico. *Ecological Monographs* **21**:379–403.
- 719 Gibbens, R., R. McNeely, K. Havstad, R. Beck, and B. Nolen. 2005. Vegetation changes in  
720 the Jornada Basin from 1858 to 1998. *Journal of Arid Environments* **61**:651–668.
- 721 Goslee, S., K. Havstad, D. Peters, A. Rango, and W. Schlesinger. 2003. High-resolution  
722 images reveal rate and pattern of shrub encroachment over six decades in New Mexico,  
723 USA. *Journal of Arid Environments* **54**:755–767.
- 724 Grover, H. D., and H. B. Musick. 1990. Shrubland encroachment in southern New Mex-  
725 ico, USA: an analysis of desertification processes in the American Southwest. *Climatic*  
726 *change* **17**:305–330.
- 727 Harrington, G. N. 1991. Effects of soil moisture on shrub seedling survival in semi-arid  
728 grassland. *Ecology* **72**:1138–1149.
- 729 Hsieh, C.-I., and G. G. Katul. 1997. Dissipation methods, Taylor’s hypothesis, and  
730 stability correction functions in the atmospheric surface layer. *Journal of Geophysical*  
731 *Research: Atmospheres* **102**:16391–16405.
- 732 Huang, H., L. D. Anderegg, T. E. Dawson, S. Mote, and P. D’Odorico. 2020. Critical tran-  
733 sition to woody plant dominance through microclimate feedbacks in North American  
734 coastal ecosystems. *Ecology* **101**:e03107.

- 735 Jongejans, E., K. Shea, O. Skarpaas, D. Kelly, and S. P. Ellner. 2011. Importance of  
736 individual and environmental variation for invasive species spread: a spatial integral  
737 projection model. *Ecology* **92**:86–97.
- 738 Katul, G., A. Porporato, R. Nathan, M. Siqueira, M. Soons, D. Poggi, H. Horn, and S. A.  
739 Levin. 2005. Mechanistic analytical models for long-distance seed dispersal by wind.  
740 *The American Naturalist* **166**:368–381.
- 741 Keitt, T. H., M. A. Lewis, and R. D. Holt. 2001. Allee effects, invasion pinning, and  
742 species' borders. *The American Naturalist* **157**:203–216.
- 743 Kelleway, J. J., K. Cavanaugh, K. Rogers, I. C. Feller, E. Ens, C. Doughty, and N. Saintilan.  
744 2017. Review of the ecosystem service implications of mangrove encroachment into  
745 salt marshes. *Global Change Biology* **23**:3967–3983.
- 746 Knapp, A. K., J. M. Briggs, S. L. Collins, S. R. Archer, M. S. BRET-HARTE, B. E. Ewers,  
747 D. P. Peters, D. R. Young, G. R. Shaver, E. Pendall, et al. 2008. Shrub encroachment in  
748 North American grasslands: shifts in growth form dominance rapidly alters control of  
749 ecosystem carbon inputs. *Global Change Biology* **14**:615–623.
- 750 Kot, M., M. A. Lewis, and P. van den Driessche. 1996. Dispersal data and the spread of  
751 invading organisms. *Ecology* **77**:2027–2042.
- 752 Lewis, M., and P. Kareiva. 1993. Allee dynamics and the spread of invading organisms.  
753 *Theoretical Population Biology* **43**:141–158.
- 754 Lewis, M. A., M. G. Neubert, H. Caswell, J. S. Clark, and K. Shea, 2006. A guide to cal-  
755 culating discrete-time invasion rates from data. Pages 169–192 *in* Conceptual ecology  
756 and invasion biology: reciprocal approaches to nature. Springer.



- 757 Mabry, T. J., J. H. Hunziker, D. Difeo Jr, et al. 1978. Creosote bush: biology and chemistry  
758 of *Larrea* in New World deserts. Dowden, Hutchinson & Ross, Inc.
- 759 Maddox, J. C., and S. Carlquist. 1985. Wind dispersal in Californian desert plants:  
760 experimental studies and conceptual considerations. *Aliso: A Journal of Systematic*  
761 *and Evolutionary Botany* **11**:77–96.
- 762 Moore, D., and K. Hall, 2022. Meteorology Data from the Sevilleta Na-  
763 tional Wildlife Refuge, New Mexico. Environmental Data Initiative.  
764 <https://doi.org/10.6073/pasta/d56307b398e28137dabaa6994f0f5f92>.
- 765 Moreno-de las Heras, M., L. Turnbull, and J. Wainwright. 2016. Seed-bank structure  
766 and plant-recruitment conditions regulate the dynamics of a grassland-shrubland Chi-  
767 huahuan ecotone. *Ecology* **97**:2303–2318.
- 768 Mugasi, S., E. Sabiiti, and B. Tayebwa. 2000. The economic implications of bush en-  
769 croachment on livestock farming in rangelands of Uganda. *African Journal of Range*  
770 *and Forage Science* **17**:64–69.
- 771 Nathan, R., G. G. Katul, G. Bohrer, A. Kuparinen, M. B. Soons, S. E. Thompson, A. Trakht-  
772 enbrot, and H. S. Horn. 2011. Mechanistic models of seed dispersal by wind. *Theoret-*  
773 *ical Ecology* **4**:113–132.
- 774 Neubert, M. G., and H. Caswell. 2000. Demography and dispersal: calculation and  
775 sensitivity analysis of invasion speed for structured populations. *Ecology* **81**:1613–  
776 1628.
- 777 Oba, G., E. Post, P. Syvertsen, and N. Stenseth. 2000. Bush cover and range condition  
778 assessments in relation to landscape and grazing in southern Ethiopia. *Landscape*  
779 *ecology* **15**:535–546.

- 780 Obrist, D., and J. Arnone Iii. 2003. Increasing CO<sub>2</sub> accelerates root growth and enhances  
781 water acquisition during early stages of development in *Larrea tridentata*. *New Phytologist* **159**:175–184.  
782
- 783 Pan, S., and G. Lin. 2012. Invasion traveling wave solutions of a competitive system with  
784 dispersal. *Boundary Value Problems* **2012**:120.
- 785 Parizek, B., C. M. Rostagno, and R. Sottini. 2002. Soil erosion as affected by shrub  
786 encroachment in northeastern Patagonia. *Rangeland Ecology & Management/Journal*  
787 *of Range Management Archives* **55**:43–48.
- 788 Peters, D. P., and J. Yao. 2012. Long-term experimental loss of foundation species:  
789 consequences for dynamics at ecotones across heterogeneous landscapes. *Ecosphere*  
790 **3**:1–23.
- 791 Petrie, M., S. Collins, D. Gutzler, and D. Moore. 2014. Regional trends and local variability  
792 in monsoon precipitation in the northern Chihuahuan Desert, USA. *Journal of*  
793 *Arid Environments* **103**:63–70.
- 794 Ratajczak, Z., J. B. Nippert, and S. L. Collins. 2012. Woody encroachment decreases  
795 diversity across North American grasslands and savannas. *Ecology* **93**:697–703.
- 796 Ratajczak, Z., J. B. Nippert, J. C. Hartman, and T. W. Ocheltree. 2011. Positive feedbacks  
797 amplify rates of woody encroachment in mesic tallgrass prairie. *Ecosphere* **2**:1–14.
- 798 Raupach, M. 1994. Simplified expressions for vegetation roughness length and zero-  
799 plane displacement as functions of canopy height and area index. *Boundary-Layer*  
800 *Meteorology* **71**:211–216.
- 801 Ravi, S., P. D’Odorico, S. L. Collins, and T. E. Huxman. 2009. Can biological invasions  
802 induce desertification? *The New Phytologist* **181**:512–515.

- 803 Reed, M., L. Stringer, A. Dougill, J. Perkins, J. Atlhopheng, K. Mulale, and N. Favretto.  
804 2015. Reorienting land degradation towards sustainable land management: Linking  
805 sustainable livelihoods with ecosystem services in rangeland systems. *Journal of envi-  
806 ronmental management* **151**:472–485.
- 807 Reynolds, J. F., R. A. Virginia, P. R. Kemp, A. G. De Soyza, and D. C. Tremmel. 1999.  
808 Impact of drought on desert shrubs: effects of seasonality and degree of resource  
809 island development. *Ecological Monographs* **69**:69–106.
- 810 Rogers, H. S., N. G. Beckman, F. Hartig, J. S. Johnson, G. Pufal, K. Shea, D. Zurell, J. M.  
811 Bullock, R. S. Cantrell, B. Loiselle, et al. 2019. The total dispersal kernel: a review and  
812 future directions. *AoB Plants* **11**:plz042.
- 813 Roques, K., T. O’connor, and A. R. Watkinson. 2001. Dynamics of shrub encroachment in  
814 an African savanna: relative influences of fire, herbivory, rainfall and density depen-  
815 dence. *Journal of Applied Ecology* **38**:268–280.
- 816 Schlesinger, W. H., and A. M. Pilmanis. 1998. Plant-soil interactions in deserts. *Biogeo-  
817 chemistry* **42**:169–187.
- 818 Schlesinger, W. H., J. A. Raikes, A. E. Hartley, and A. F. Cross. 1996. On the spatial  
819 pattern of soil nutrients in desert ecosystems: ecological archives E077-002. *Ecology*  
820 **77**:364–374.
- 821 Schlesinger, W. H., J. F. Reynolds, G. L. Cunningham, L. F. Huenneke, W. M. Jarrell, R. A.  
822 Virginia, and W. G. Whitford. 1990. Biological feedbacks in global desertification.  
823 *Science* **247**:1043–1048.
- 824 Sirami, C., and A. Monadjem. 2012. Changes in bird communities in Swaziland savannas

825 between 1998 and 2008 owing to shrub encroachment. *Diversity and Distributions*  
826 **18**:390–400.

827 Skarpaas, O., and K. Shea. 2007. Dispersal patterns, dispersal mechanisms, and invasion  
828 wave speeds for invasive thistles. *The American Naturalist* **170**:421–430.

829 Stephens, P. A., W. J. Sutherland, and R. P. Freckleton. 1999. What is the Allee effect?  
830 *Oikos* pages 185–190.

831 Sullivan, L. L., B. Li, T. E. Miller, M. G. Neubert, and A. K. Shaw. 2017. Density depen-  
832 dence in demography and dispersal generates fluctuating invasion speeds. *Proceed-*  
833 *ings of the National Academy of Sciences* **114**:5053–5058.

834 Taylor, C. M., and A. Hastings. 2005. Allee effects in biological invasions. *Ecology Letters*  
835 **8**:895–908.

836 Thompson, S. E., S. Assouline, L. Chen, A. Trahktenbrot, T. Svoray, and G. G. Katul. 2014.  
837 Secondary dispersal driven by overland flow in drylands: Review and mechanistic  
838 model development. *Movement ecology* **2**:7.

839 Trollope, W., F. Hobson, J. Danckwerts, and J. Van Niekerk. 1989. Encroachment and  
840 control of undesirable plants. *Veld management in the Eastern Cape* pages 73–89.

841 Turnbull, L., J. Wainwright, and R. E. Brazier. 2010. Changes in hydrology and erosion  
842 over a transition from grassland to shrubland. *Hydrological Processes: An Interna-*  
843 *tional Journal* **24**:393–414.

844 Van Auken, O. 2009. Causes and consequences of woody plant encroachment into  
845 western North American grasslands. *Journal of environmental management* **90**:2931–  
846 2942.

- 847 Van Auken, O. W. 2000. Shrub invasions of North American semiarid grasslands. Annual  
848 review of ecology and systematics **31**:197–215.
- 849 Vasek, F. C. 1980. Creosote bush: Long-lived clones in the Mojave Desert. American  
850 Journal of Botany **67**:246–255.
- 851 Veit, R. R., and M. A. Lewis. 1996. Dispersal, population growth, and the Allee effect: dy-  
852 namics of the house finch invasion of eastern North America. The American Naturalist  
853 **148**:255–274.
- 854 Wang, M.-H., M. Kot, and M. G. Neubert. 2002. Integrodifference equations, Allee effects,  
855 and invasions. Journal of mathematical biology **44**:150–168.
- 856 Weber-Grullon, L., L. Gherardi, W. A. Rutherford, S. R. Archer, and O. E. Sala. 2022.  
857 Woody-plant encroachment: Precipitation, herbivory, and grass-competition interact  
858 to affect shrub recruitment. Ecological Applications **32**:e2536.
- 859 Wiernga, J. 1993. Representative roughness parameters for homogeneous terrain.  
860 Boundary-Layer Meteorology **63**:323–363.
- 861 Wilcox, B. P., A. Birt, S. D. Fuhlendorf, and S. R. Archer. 2018. Emerging frameworks for  
862 understanding and mitigating woody plant encroachment in grassy biomes. Current  
863 Opinion in Environmental Sustainability **32**:46–52.
- 864 Williams, J. L., T. E. Miller, and S. P. Ellner. 2012. Avoiding unintentional eviction from  
865 integral projection models. Ecology **93**:2008–2014.
- 866 Wood, S. 2017. Generalized Additive Models: An Introduction with R. 2 edition. Chap-  
867 man and Hall/CRC.

## Appendix A: Dispersal kernel modeling

*WALD dispersal kernel.* In order to create the dispersal kernel, we first take the wind speeds at measurement height  $z_m$  and correct them to find wind speed  $U$  for any height  $H$  by using the logarithmic wind profile.

$$U = \frac{1}{H} \int_{d+z_0}^H \frac{u^*}{K} \log \left( \frac{z-d}{z_0} \right) dz \quad (\text{A1})$$

given in Bullock et al. (2012) equation 6, with the notation slightly modified. Here,  $z$  is the height above the ground,  $K$  is the von Karman constant, and  $u^*$  is the friction velocity. The zero-plane displacement  $d$  and roughness length  $z_0$  are surface roughness parameters that, for a grass canopy height  $h$  above the ground, are approximated by  $d \approx 0.7h$  and  $z_0 \approx 0.1h$ . These estimates are from Raupach (1994) for a canopy area index  $\Lambda = 1$  in which the sum of grass canopy elements is equal to the unit area being measured. A 0.15 m grass height at our study site gives  $d = 0.105$  and  $z_0$ , which are suitable approximations for grassland (Wiernga, 1993). Calculations of  $u^*$  were done using equation A2 from Skarpaas and Shea (2007), in which

$$u^* = KU_m \left[ \log \left( \frac{z_m - d}{z_0} \right) \right]^{-1} \quad (\text{A2})$$

and  $U_m$  is the mean wind velocity at the measurement height  $z_m$ . Values for the turbulent flow parameter  $\sigma$  were then calculated using the estimate made by Skarpaas and Shea (2007) in their equation A4, where

$$\sigma = 2A_w^2 \sqrt{\frac{K(z-d)u^*}{C_0U}} \quad (\text{A3})$$

and  $C_0$  is the Kolmogorov constant.  $A_w$  is a constant that relates vertical turbulence

to friction velocity and is approximately equal to 1.3 under the assumptions of above-canopy flow made by Skarpaas and Shea (2007), based off calculations from Hsieh and Katul (1997). We used maximum plant height  $H$  as a measure of  $z$ .

The values from the previous three equations give us the necessary information to calculate  $\mu'$  and  $\lambda'$ , thus allowing us to create the WALD distribution  $p(r)$ . However, the base WALD model does not take into account variation in wind speeds or seed terminal velocities, which limits its applicability in systems where such variation is present. In order to account for this variation, we integrate the WALD model over distributions of these two variables using the same method as Skarpaas and Shea (2007). Additionally, the WALD model assumes seed release from a single point source, which is not realistic for creosote bush; because seeds are released across the entire height of the shrub rather than from a point source, we integrated  $p(r)$  across the uniform distribution from the grass canopy height to the shrub height. Thus, under the assumptions that the height at which a seed is located does not affect its probability of being released and that seeds are evenly distributed throughout the shrub, this gives the dispersal kernel  $K(r)$ , where

$$K(r) = \iiint p(F)p(U)p(z)p(r) dF dU dz \quad (\text{A4})$$

and  $p(F)$  and  $p(U)$  are the PDFs of the terminal velocity  $F$  and wind speed  $U$ , respectively, and  $p(z)$  is the uniform distribution from  $h$  to  $H$ .

*Dispersal data collection.* The distribution  $p(F)$  in the integral above was constructed using experimentally determined seed terminal velocities. This was done by using laboratory-based seed release experiments with a high-speed camera and motion tracking software to determine position as a function of time. We then used the Levenberg-Marquardt algorithm to solve a quadratic-drag equation of motion for  $F$ . Before seeds

911 were released, they were dried, dyed with yellow fluorescent powder, and then put  
912 against a black background to improve visibility and make tracking easier. While the  
913 powder added mass to the seeds, this added mass only yielded an approximately 2.5%  
914 increase, likely having little effect on terminal velocities. Measurements were conducted  
915 for 48 seeds that were randomly chosen from a seed pool derived from different plants,  
916 and then an empirical PDF of terminal velocities was constructed using the data. Con-  
917 structing  $p(U)$  involved creating an empirical PDF of hourly wind speeds using data  
918 from Sevilleta LTER meteorological station 49, the station closest to our transects. We  
919 used wind speed data collected hourly from 2015 to 2019 (Moore and Hall, 2022).



## Appendix B: Additional results

Pr(Survival)	df	dAIC
~size + transplant + size:transplant + (1 transect)	11.50	1.72
~size + transplant + density + size:transplant + density:transplant + (1 transect)	13.19	0.19
~size + transplant + density + size:transplant + density:transplant + size:density + size:transplant:density + (1 transect)	14.22	0.00

Table B1: AIC model selection for survival probability.

mean(size)	sd(size)	df	dAIC
~size + (1 transect)	~1	3.00	1024.88
~size + density + (1 transect)	~1	8.50	977.23
~size + density + size:density + (1 transect)	~1	10.47	975.17
~size + (1 transect)	~size	9.65	146.23
~size + density + (1 transect)	~size	16.24	19.45
~size + density + size:density + (1 transect)	~size	18.55	19.62
~size + (1 transect)	~size + density	10.40	115.52
~size + density + (1 transect)	~size + density	18.97	0.08
~size + density + size:density + (1 transect)	~size + density	21.33	0.00

Table B2: AIC model selection for mean and variance of future size

Pr(Flowering)	df	dAIC
~size + (1 transect)	5.78	0.63
~size + density + (1 transect)	6.80	2.32
~size + density + size:density + (1 transect)	7.24	0.00

Table B3: AIC model selection for flowering probability.

No. fruits	df	dAIC
$\sim \text{size} + (1 \text{transect})$	14.25	71.99
$\sim \text{size} + \text{density} + (1 \text{transect})$	5.52	0.00
$\sim \text{size} + \text{density} + \text{size}:\text{density} + (1 \text{transect})$	6.23	0.37

Table B4: AIC model selection for fruit number.

Pr(Recruitment)	df	dAIC
$\sim (1 \text{transect})$	6.57	0.00
$\sim \text{density} + (1 \text{transect})$	7.39	0.93

Table B5: AIC model selection for recruitment probability.

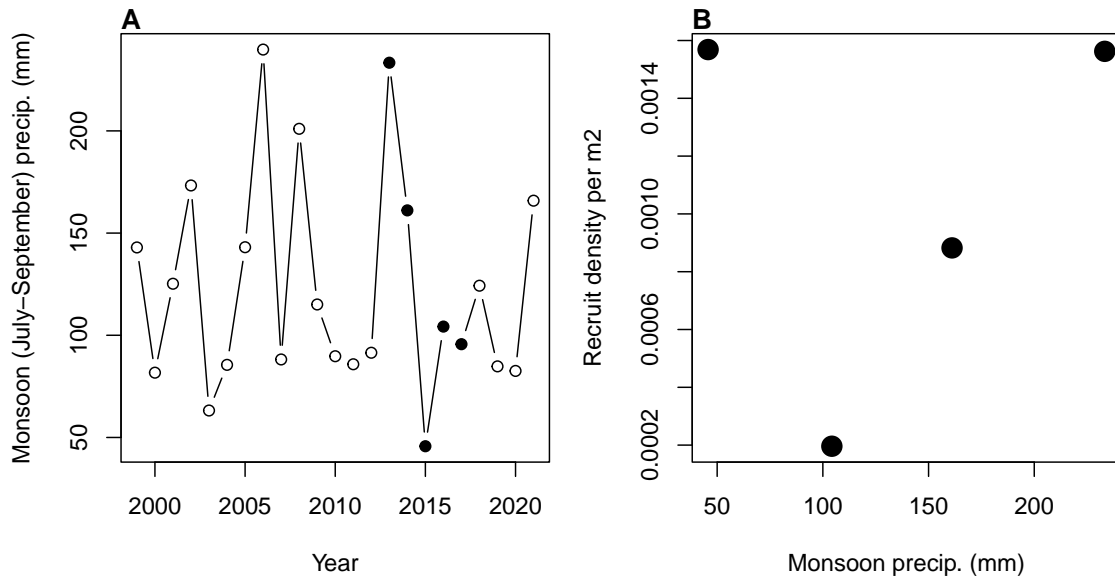


Figure B1: A, Time series of annual monsoon precipitation (filled circles are the years in which this study was conducted). B, Relationship between density of creosote recruits observed on our transects in May-June and monsoon precipitation in the preceding July-September.

mean(size)	sd(size)	df	dAIC
~(1 transect)	~1	2.00	2.90
~density+(1 transect)	~1	4.42	0.00
~(1 transect)	~density	3.00	4.74
~density+(1 transect)	~density	5.56	1.21

Table B6: AIC model selection for mean and variance of recruit size.